Invited Paper

High performance terahertz quantum cascade lasers

Y.Y. Li [1, 2], J. Q. Liu [2*, 3], F.Q. Liu [1, 2, 3] and Z. G. Wang [2, 3]

[1] Division of Quantum Materials and Devices, Beijing Academy of Quantum Information Sciences, Beijing 100193, China

[2] Key Lab. Of Semiconductor Materials Science, Institute of Semiconductor, Chinese Academy of Sciences, Beijing 100083, China

[3] Center of Materials Science and Optoelectronics Engineering, University of Chinese Academy of Sciences, Beijing, 100049, China

[*2] Email: jqliu@semi.ac.cn

(Received May 21, 2020)

Abstract: Terahertz region is the electromagnetic gap between the infrared optoelectronics and the high frequency electronics, which is of broad prospects in applications. The application requirements drive the rapid development in Terahertz technologies including sources, detectors and systems. In the last two decades, quantum cascade laser has made great progress as one of the most promising terahertz sources. In this paper, we present the development of terahertz quantum cascade lasers in our group.

Keywords: Terahertz, Quantum cascade lasers, Distributed feedback, Beam pattern

doi: https://doi.org/10.1051/tst/2020132061

1. Introduction

Terahertz (THz) spectral region is defined as 0.1-10 *THz* in the electromagnetic spectrum, a gap between infrared optoelectronics and high frequency electronics. THz region has special property of very low energy which can penetrate through many materials such as fabric and paper. Meanwhile, unlike X ray, THz is non-destructive to biological tissues. In addition, owing to the existence of rotational molecular bands, THz regime has a great value for spectroscopy. These unique properties of THz region have attracted great attention of the scientific and commercial communities. As a result, THz technologies including sources, detectors, and modulators have developed rapidly during the last two decades.

In order to make the THz applications to be true, high-power THz sources are highly desired. Photonic and electronic fields are both trying to extend their frontiers to bridge THz gap. Traditional semiconductor laser has provided compact and various choices for electromagnetic generation. However, the technology for THz radiation is limited by the bandgap between the conduction and valence bands. Different from traditional semiconductor laser, quantum cascade

laser (QCL) belongs to "intraband" laser. Since the first demonstration of THz QCL in 2002 [1], it has become one of the most potential THz sources.

2. High-power THz quantum cascade laser

2.1 What is THz quantum cascade laser?

Quantum cascade laser (QCL) is an intraband emitter，which is different from interband semiconductor laser. The core region of QCL is periodic quantum wells and barriers. Due to the existence of nanoscale barriers, quantum wells are strongly intercoupled, which results in delocalized subband wavefunctions, realizing efficient electron transition between overlapped states. The utilization of quantum well and quantum tunneling breaks the continuous conduction band into a series of semi-discrete subbands in K space and forms a string of energy levels spacing from several *meV* to hundreds of *meV* due to quantum size confinement effect in quantum well. After applying a certain external electric field, electrons flow directionally from one subband to another by emission or absorption of photons or phonons without the interplay of valance band. The schematic diagram of QCL radiation mechanism is shown in Fig.1 (a).

Since the advent of first THz QCL in 2002, steady improvements have been made in the design of active region. There are four major design classes of active structure: chirped superlattice (CSL), bound-to-continuum (BTC) design, resonant phonon (RP) scheme and a hybrid design of BTC transition combined with RP extraction. The high-power active region using in this article is a hybrid design, presented in Fig.1 (b). Thanks to the ultra-fast intrasubband LO-phonon assisted scattering process, high electrons injection efficiency to the upper laser level and high extraction efficiency to the lower could be realized, which results in population inversion in the active region.

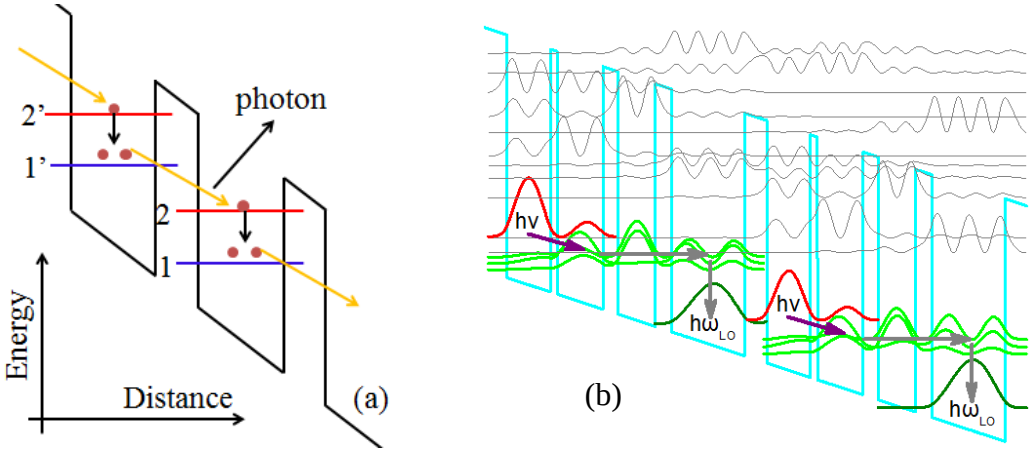

Fig. 1 (a) Schematic illustration of QCL radiation mechanism; (b) A conduction-band diagram for a hybrid THz QCL design.

2.2 High-power epitaxial-side down mounted THz QCL

Up to now, a series of QCLs with frequency from ~2.5*THz* to ~5*THz* have been grown in our group. The spectra are shown in Fig. 2. Compared with metal-metal (MM) waveguide, THz QCL with semi-insulating surface-plasma (SISP) waveguide can provide high output power due to their spatially extended transverse mode profile. The low optical confinement factor r≈0.1–0.5 of SISP waveguide produces a low-divergence beam as well as low-reflectivity (R≈0.32) output facet, making mirror loss comparable with waveguide loss. In 2014, pulsed power of ~1*W* has been achieved from SISP THz QCLs [2]. However, the performance is still affected seriously by the poor heat removal ability in the active core region. Consequently, improving the thermal management is vital to produce high-power THz QCLs. In 2016, our group presented an epitaxial-side down (Epi-down) mounting scheme [3, 4] in coplanar waveguide for SISP THz QCL to enhance the heat extraction ability from the active region. High output power and high wall-plug efficiency were realized in wide ridge lasers with a single-lobe horizontal beam pattern.

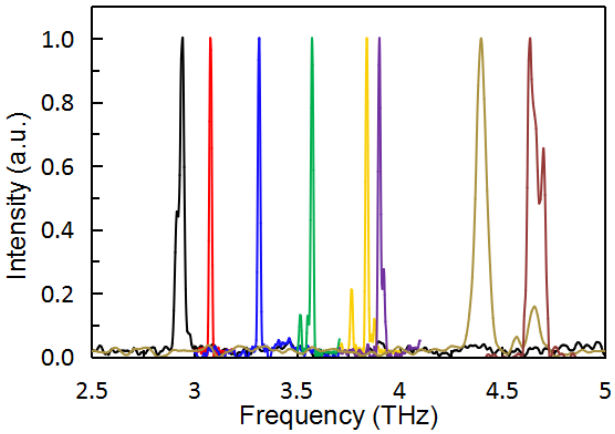

Fig. 2 Spectra of representative THz QCLs grown in our group.

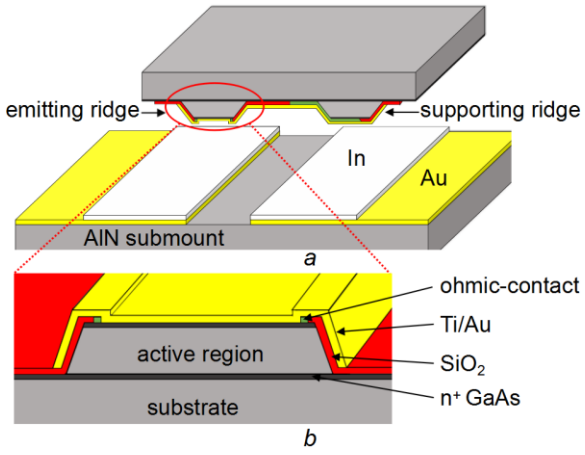

Fig. 3 Details of Epi-down laser [4].

Different from Epi-up mounted lasers, an extra ridge was defined adjacent to the light emitting ridge as an injection electrode to facilitate Epi-down bonding as shown in Fig. 3 [4]. In order to quantitatively explain the heat removal ability of THz QCLs, two-dimensional heat flow distributions for devices with different structures have been simulated by a finite-element electromagnetic solver (COMSOL). In these simulations, two kinds of mounting structures were assumed, the non-Au-electroplated Epi-up and the Au-electroplated Epi-down. The ridge width of THz QCLs was set to 500 μm. As shown in Fig. 4, at the same heat-sink temperature of 90 K, the highest active region temperatures for the two type lasers are 151 K and 141 K, respectively. The peak temperature of the Epi-up mounted laser is approximately 10 K higher than that of the Epi-down structure with Au-electroplating profile. It is evident that the Epi-down mounted structure improves the heat removal ability of the active region and thus raises the output power and the maximum operating temperature.

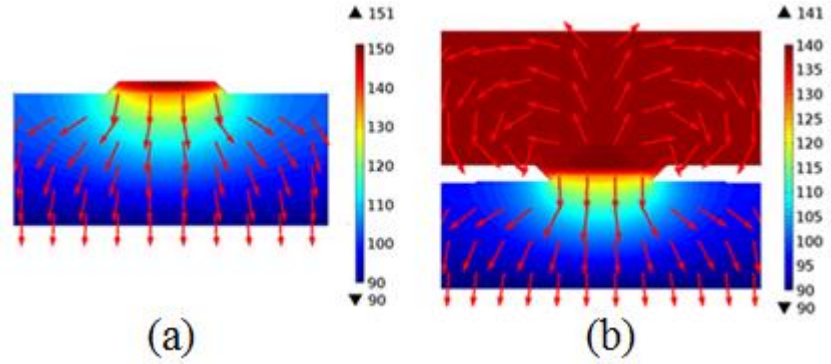

Fig. 4 Nonlinear finite-element solver calculated two-dimensional heat flow. The temperature of heat-sinks was set to be 90K. (a) Epi-up mounted laser; (b) Au-electroplated Epi-down mounted laser.

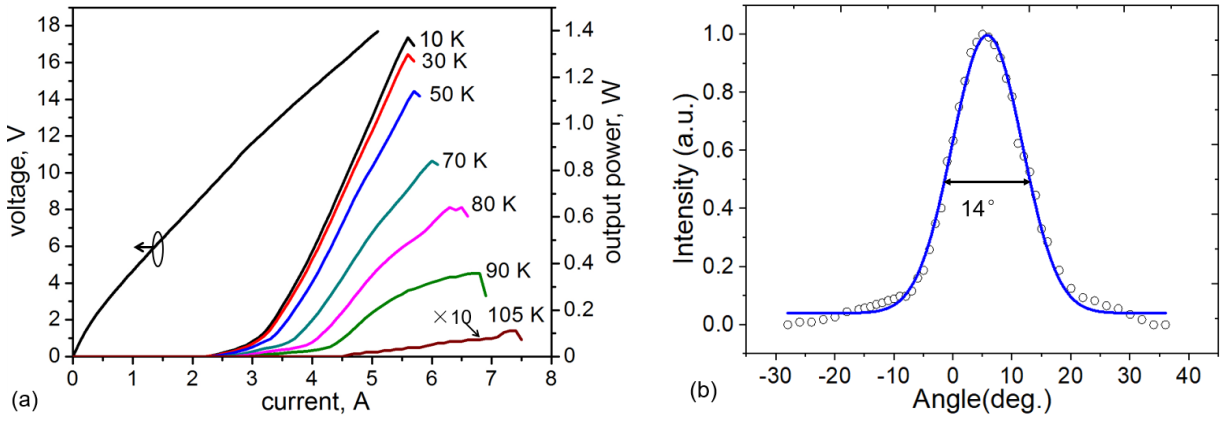

Fig. 5 (a) Light against current, (b) horizontal beam pattern from a 500-μm-wide and 4-mm-long Epi-down mounted device in pulsed mode.

Fig. 5(a) shows the light–current curves from a 500μm × 4mm Epi-down mounted laser measured at various heat-sink temperatures [4]. At 10K, a peak output power of 1.37W from both facets is obtained with a slope efficiency about 570mW/A. Fig. 5(b) illustrates the horizontal beam pattern of the QCL at the front facet. A single-lobe with a full-width at half-maximum (FWHM) divergence angle of 14° is realized, even though the ridge width is much larger than the wavelength in the active region. In THz QCL, except for the fundamental lateral mode, high-order modes always locate at both sides of the ridge. In our devices, two narrow Ohmic contact stripes were fabricated at the top of the ridge edges, which increase the absorption loss of the high-order lateral modes. Additionally, the SiO_2 layer deposited at the side walls of the ridge also increases the loss of the high-order modes.

2.3 THz QCL coupled with lens

Although SISP waveguide laser features high power due to the low optical confinement, the limited area of output facet leads to a divergent beam pattern exceeding 40°along the material growth direction. In MM device, various technologies have been studied to integrate photonic microstructures [5-8] with THz QCL for realizing surface emission and reducing beam divergence. But these methods are not suitable for SISP devices owing to the low surface extraction efficiency. Alternately, SISP waveguide with a dielectric lens can be used to improve the beam pattern. Silicon lens is an appropriate choice for which refractive index is ~3.4, matching to the GaAs active region ~3.6.

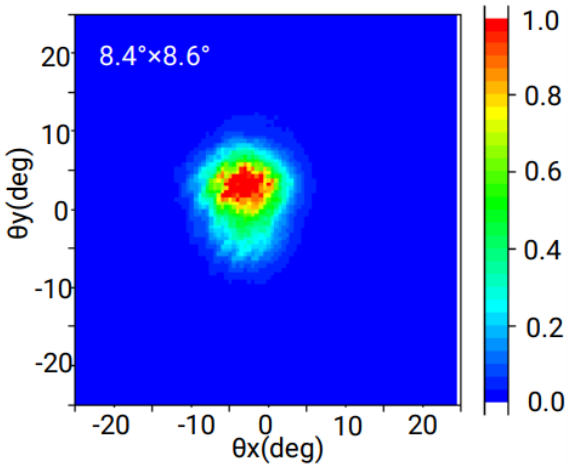

Fig. 6 The measured far-field beam pattern of a 150-μm-wide SISP laser coupled with a Si lens.

The diameter of the silicon lens we presented here is 3mm with a total length of 1.96mm. When the lens is placed in contact with the output facet of 150-μm-wide laser, the simulated divergence angle of far-field pattern is ~8.7°. Special copper heat sinks were designed to integrate laser and lens. The device was measured in a Dewar under liquid-nitrogen temperature (77K). The far-field beam pattern at peak power has a divergence degree of 8.4°×8.6° as shown in Fig.6， which

agrees with the simulation result. Silicon lens with larger diameter could further decrease the divergence of beam pattern.

3. Single-mode THz quantum cascade laser

Distributed feedback (DFB) is a reliable compact approach in THz QCL to realize coherent single-mode emission. For various applications such as THz spectroscopy, wireless communication, and remote sensing technology, good emission characteristics of not only stable single-mode, but also high output power and well-shaped beam pattern are desired. Consequently, DFB THz QCLs fabricated with different structures and methods have been presented in the past years. According to the waveguides, two different technical routes are formed for single-mode THz QCLs, i.e. SISP edge-emitting and MM surface-emitting. The MM surface-emitting THz QCL is often realized by incorporating high-order DFB grating [9-13], which is advantageous for the directional beam pattern and high beam quality. However, the output power is limited severely by the grating coupling mechanism that the radiation perpendicular to the plane is provided by the first-order diffraction of the high-order DFB grating while the feedback parallel to the plane is offered by the second-order diffraction.

Compared with MM waveguide structure, SISP DFB THz QCL, in which the radiation and feedback are both provided by the first-order diffraction of the first-order grating, features high output power and enables relatively wide ridge without supporting multiple transverse modes due to the infiltration of light field into the substrate. Nevertheless, there still exists issues for its further power enhancement by only increasing cavity size. We optimized SISP single-mode lasers with two approaches.

3.1 Tapered single-mode THz quantum cascade laser

Increasing the width of laser ridge is the most direct way to get high power for DFB lasers. However, simply widening the laser ridge leads to high-order transverse mode operation and then results in poor beam quality. Master oscillator-power amplifier (MOPA) structure [14-16] is a good choice for achieving high power while maintaining fundamental mode emission. In this structure, stable single-mode emission can be obtained when self lasing of the PA section is suppressed. This is usually achieved by cleaving the front facet at a small angle [14] or by depositing an antireflection (AR) coating layer on the front facet [15, 17]. However, due to the long wavelength, AR coating is so difficult for THz QCL [18]. In addition, separate electrical pumping for the seed and amplifier sections is request for MOPA devices, which is inconvenient for testing and applications. Different form MOPA, tapered structure is more convenient [19] which requires only a single top contact and the laser oscillation takes place in the whole cavity. The short straight section is designed narrow enough to select the fundamental transverse mode

TM_{00} for good beam pattern as well as the large area tapered section is used to broaden the gain area for higher output power while reducing the power density and suppressing the catastrophic optical damage of the output facet.

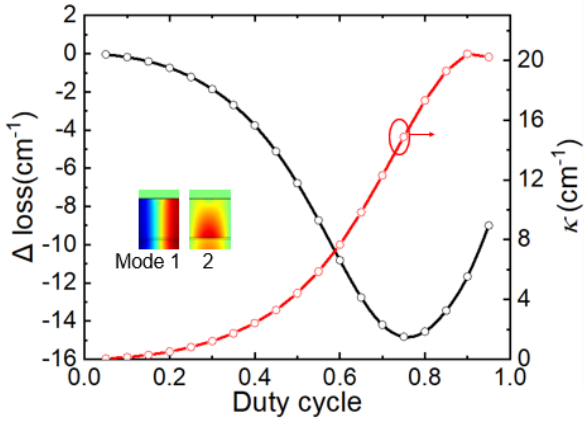

Fig. 7 Waveguide loss difference between the first two modes and coupling coefficient against duty cycle with fixed etch depth.

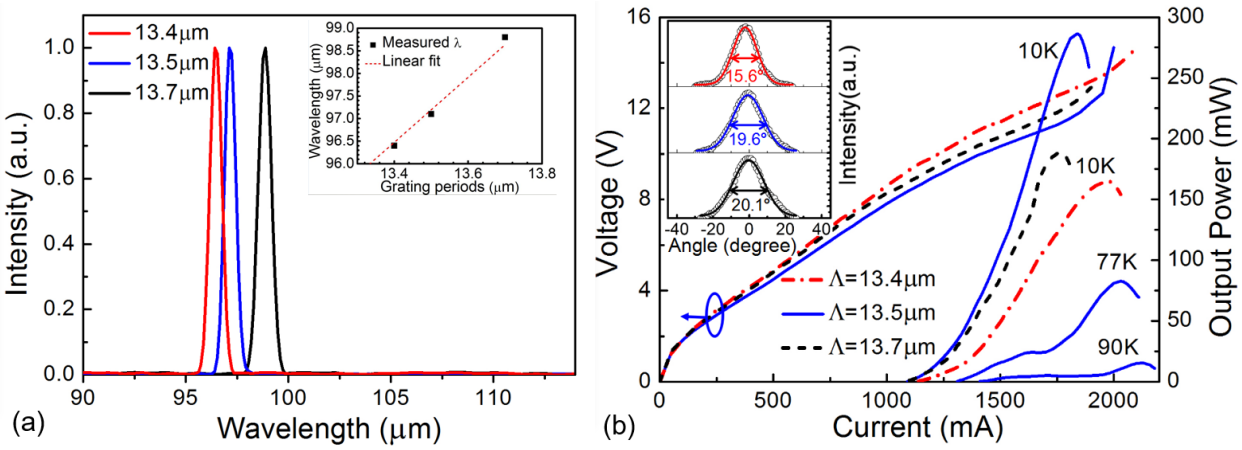

Fig. 8 (a) Lasing spectra, (b)output power and beam pattern with different grating periods.

We made tapered DFB THz QCLs with grating periods of 13.4, 13.5, and 13.7μm, which were defined due to calculated effective index 3.6 and central wavelength ~97μm. To obtain stable single mode, the surface grating structure has been simulated to optimize the duty cycle for large waveguide loss difference and moderate grating coupling coefficient κ. The simulation was based on COMSOL with periodical boundary conditions. The results are plotted in Fig.7 with a constant grating depth and a variable grating duty cycle ε. As shown in Fig.7, the loss of mode 1 is always lower than that of mode 2, and the loss difference between the first two modes gets the maximum value at ε=0.75. Besides, with duty cycle increases, the coupling coefficient increases gradually and gets the maximum value at ε=0.9. Considering a compromise between coupling coefficient and waveguide loss, 11.5-μm-wide metallic-stripes were selected. Therefore, duty cycles of 85.8, 85.2, and 84% were obtained corresponding to grating periods Λ=13.4μm, 13.5 μm, and 13.7μm, respectively.

The narrow straight ridge is 0.5-*mm*-long with a width of 200μm, which is narrow enough for selecting fundamental mode. The tapered ridge is 2.5-*mm*-long and characterized with a taper half-angle θ of 2.5°. The normalized spectra for tapered DFB lasers are displayed in Fig. 8 (a), which were measured at nearly maximum output power. Central wavelength of 96.4, 97.1, and 98.8μm are obtained for different grating periods (13.4, 13.5, 13.7*um*), respectively. Stable single-mode operation is realized under all testing conditions with a SMSR of 25*dB*. A good linear relationship between spectra and grating periods is exhibited in the inset of Fig. 8(a). The maximum emission powers are 165, 286, and 188*mW* for lasers of Λ=13.4μm, 13.5μm, and 13.7μm, respectively, at 10*K*. The difference of peak output power among these lasers with different grating periods originates from the location of Bragg wavelength in the gain spectrum. The inset of Fig. 8(b) displays the horizontal beam patterns of the three lasers. Single-lobe beam patterns are obtained due to the fundamental mode selection effect of the narrow straight section and the existence of high-loss boundary conditions. Gaussian fitted curves of measured normalized intensity show the FWHM divergence angles of 15.6°, 19.6°, and 20.1°.

3.2 Sampled grating THz quantum cascade laser

For improving output power of DFB THz QCL, in addition to the deteriorative beam pattern, there exists another issue that the output power is always restricted by the over-coupled mechanism [21] in long cavity lasers. In this kind of DFB mechanism, larger coupling strength (κ L), leads to more light reflection by the DFB grating. This results in an optical field accumulates in the center of the laser and an edge-emitting attenuation from the end facets. Thus, a proper coupling strength regulation is necessary for the single-mode output power enhancement for SISP DFB QCL. We presented a sampled grating technology in SISP edge-emitting THz QCL for power scaling up [22].

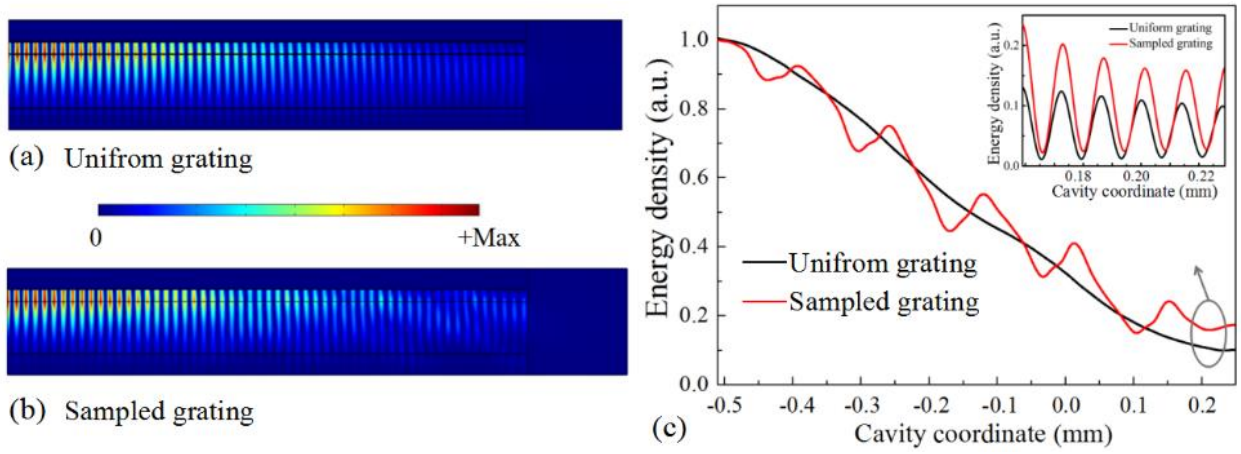

Fig. 9 The energy density distribution of the lasing mode inside 1.6-mm-long (a) uniform grating structure and (b) sampled grating structure with sampling duty cycle of 60%. Only half of the structure is simulated for saving computational memory. (c) The envelopes of normalized energy density intensity inside 1.6-*mm*-long uniform grating structure and sampled grating structure. The inset shows the detail of the energy density distribution near the lasing facet.

The effect of coupling strength on the lasing mode distribution in the grating lasers was first investigated. According the central wavelength and the calculated effective index, the uniform grating period Λ of 13.5μm was chosen. And the grating duty cycle of ε = 85% was selected to ensure the non-radiative mode being the only lasing longitude mode with a large coupling coefficient and low waveguide loss. For the sampled grating structure, sampling period Z is defined by the function $Z = \lambda_0^2 / 2\, n_{eff} (\lambda_0 - \lambda_{-1})$, where λ_{-1} is the -1 order supermode wavelength. Single-mode operation can be achieved by choosing a small period Z so that the ±1 order supermodes are shifted from the gain curve. Different sampling duty cycles ($\sigma = D/Z$) with a fixed sampling period Z and variable grating region lengths D were designed to change the effective coupling coefficient κ_{eff} which can be extracted by $\kappa_{eff} = \sigma \kappa$ simply (κ is the coupling coefficient of the uniform grating structure). This method enables almost precisely controllable variations of the coupling coefficient in axial direction of the waveguide with a simple fabrication process. Figure 9(a) and 9(b) show the energy density distribution along the cross-section of 1.6-*mm*-long uniform grating device and sampled grating device (σ = 60%) for the lasing mode, respectively [22]. To save computational memory, only half of the structure was taken into account with a perfect electronic conductor (PEC) boundary condition at the center and an absorbing boundary condition at the end facet. The simulated envelopes of the normalized energy density along cavities are presented in Figure 9(c), where the energy density at the center keeps the same. For sampled grating structure, the non-slits region forms a "FP-like" cavity. The interface reflection between slits region and non-slits region in a sampling period induces a localized energy density concentration effect along the device although the overall downwards trend. The inset of Fig. 9(c) shows a detail of the energy density distribution near the end facet. While the normalized energy density inside uniform grating laser is lower than 13% of the peak energy density, it still maintains larger than 17% inside sampled grating laser. This can be explained by the lower coupling strength of sampled grating laser while the cavity facet effect is similar for the two types of structure. Therefore, the output power of sampled grating laser would be higher than that of uniform grating laser because of the larger energy density intensity distribution near the end facet. With the increasing of the cavity length, the advantage of sampled grating laser would be more obvious. At the same time, lower waveguide loss of sampled grating laser also enhances the net optical gain.

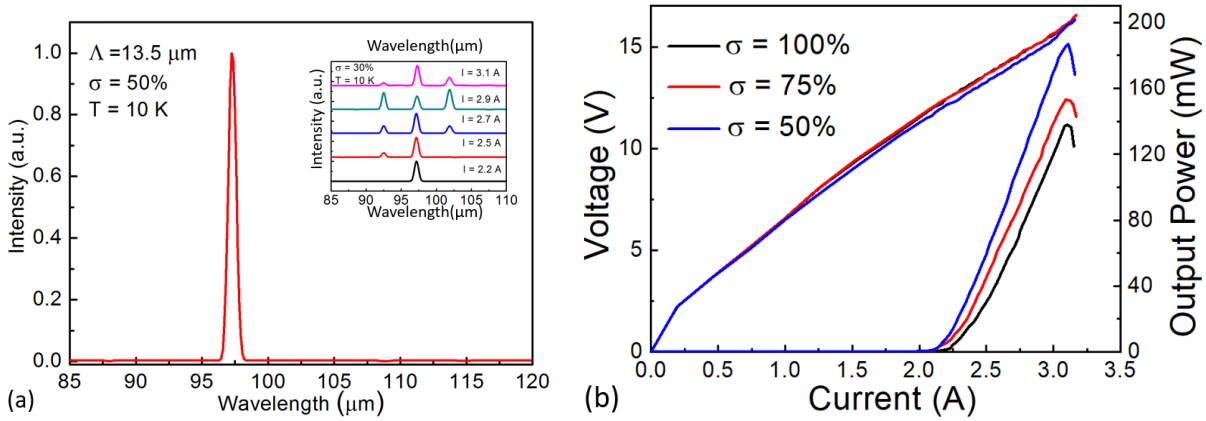

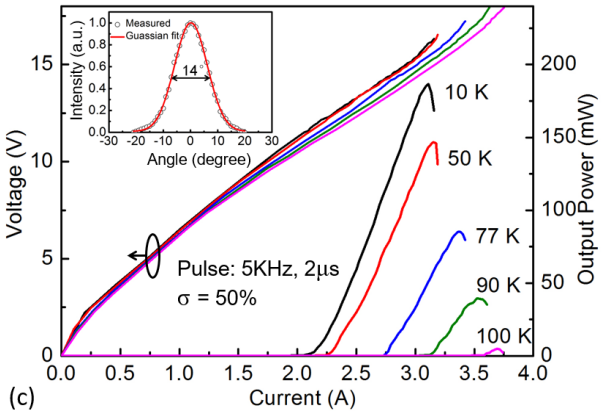

Fig. 10 (a) The emission spectrum of the sampled grating device with σ = 50% at peak output power and 10*K*. The inset shows the lasing spectra for the σ = 30% device at different injection currents. (b) Typical light-current-voltage curves for the 3-*mm*-long single-mode sampled grating devices at 10*K* with different sampling duty cycles from 100% to 50%. (c) The output characteristics of the σ = 50% device at different temperatures.

For 400-μm-wide and 3-mm-long devices, different sampling duty cycles of σ=100%, 75%, 50% and 30% were fabricated. Stable single-mode emission is realized for devices of σ=100%, 75%, 50% under all operating conditions. Fig. 10(a) shows the normalized lasing spectrum of the device with σ=50% at 10*K*. The device lases at 97.25μm with a SMSR of ~30*dB*. However, for the device with σ=30%, single-mode emission is only obtained at low currents. With the increasing of currents and temperatures, ±1st supermodes appear gradually. The mode distance fits perfectly with the calculated value. Fig. 10(b) shows the output power of the single-mode devices. A peak power of 138*mW* is obtained from the uniform grating (σ=100%) device with a threshold current density of 176A/cm^2. For sampled grating QCLs with σ=75% and 50%, the results are 153*mW* (171A/cm^2) and 186*mW* (161A/cm^2), respectively. The peak power is about 1.1 and 1.35 *times* of the uniform grating device. At the same time, the slope-efficiency is increased from 185.5*mW*/A for uniform grating to 220.7*mW/A* for σ=50%. Figure 10(c) shows the output characteristics of the device with σ = 50% at different temperatures. The output powers here were the actual measured values without being corrected by the transmission coefficient of the PE window and the optical collection efficiency of the apparatus. A maximum work temperature of 100*K* and a nearly single-lobe beam pattern with horizontal FWHM value of 14° is obtained.

5. Conclusions

In conclusion, we have reviewed the recent progress of THz QCL in our group. Epi-down mounted technology, external Si lens, tapered waveguide and sampled grating were designed to further increase the emission power of edge-emitting lasers. The rapid development of monolithic high-power THz QCL with good beam pattern will find wide applications in remote sensing, high

resolution spectroscopy, high speed communication and so on. It is hopeful and necessary to bring more technologies to THz QCL.

Acknowledgements

This work was supported in part by the National Key R&D Program of China Grant No. 2016YFB0402303, National Natural Science Foundation of China Grant No. 61734006, 61674144, 61774146, Key Program of the Chinese Academy of Sciences Grant No. QYZDJ-SSW-JSC027, XDB43000000. The authors would like to thank Ping Liang, Ying Hu for their help in the processing.

References

[1] R. Kohler, A. Tredicucci, F. Beltram, et al.. "Terahertz semiconductor heterostructure laser". *Nature*, 417, 156-159 (2002).

[2] L. H. Li, L. Chen, J. X. Zhu, et al.. "Terahertz quantum cascade lasers with ＞1W output powers". *Electron. Lett.*, 50, 309-311(2014).

[3] O. Krüger, S. Kreutzmann, D. Prasai, et al.. "Epitaxial-side mounting of terahertz quantum lasers for improved heat management". *IEEE Photon. Technol. Lett.*, 25, 1570–1573(2013).

[4] Y. Y. Li, T. wang, S. Q. Zhai, et al.. "High-power epitaxial-side down mounted terahertz quantum cascade lasers". *Electron. Lett.*, 52, 1401-1402(2016).

[5] S. Kumar, B. S. Williams, Q. Qin, et al.. "Surface-emitting distributed feedback terahertz quantum-cascade lasers in metal-metal waveguides". *Opt. Express*.15, 113-128 (2007).

[6] M. S. Vitiello, M. Nobile, A. Ronzani, et al.. "Photonic quasi-crystal terahertz lasers". *Nat. Commu*. 5, 5884-5891(2014).

[7] Y. Halioua, G. Xu, S. Moumdji, et al.. "THz quantum cascade lasers operating on radiative modes of 2D photonic crystal". *Opt. Lett*., 39, 3962-3965 (2014).

[8] C. Z. Wu, Y. Jin, J. L. Reno, et al.. "Large static tuning of narrow-beam terahertz plasmonic lasers operating at 78 K". *APL Photonics*, 2, 026101 (2016).

[9] J. A. Fan, M. A. Belkin, and F. Capasso. "Surface emitting terahertz quantum cascade laser with a double-metal waveguide". *Opt. Express*, 14, 11672-11680 (2006).

[10] G. Y. Xu, R. Colombelli, S. P. Khanna, et al.. "Efficient power extraction in surface-emitting semiconductor lasers using graded photonic heterostructures". *Nature Commu.*, 3, 952 (2012).

[11] Y. Jin, L. Gao, J. Chen, et al.. "High power surface emitting terahertz laser with hybrid second- and fourth-order Bragg gratings". *Nature Commu.*, 9, 1407 (2018).

[12] T. Y. Kan, Q. Hu and J. L. Reno. "Perfectly phase-matched third-order distributed feedback terahertz quantum-cascade lasers". *Opt. Lett*., 37, 2070-2072 (2012).

[13] H. Zhu, F. F. Wang, Q. Yan, et al.. "Terahertz master-oscillator power-amplifier quantum cascade lasers". *Appl. Phys. Lett*., 109, 231105 (2016).

[14] M. Troccoli, C. Gmachl, F. Capasso, et al.. "Mid-infrared (lambda approximate to 7.4 mu m) quantum cascade laser amplifier for high power single-mode emission and improved beam quality". *Appl. Phys. Lett*., 80, 4103-4105(2002).

[15] P. Rauter, S. Menzel, A. K. Goyal, et al.. "Master-oscillator power-amplifier quantum cascade laser array". *Appl. Phys. Lett*., 101, 261117 (2012).

[16] H. Zhu, H. Q. Zhu, F. F. Wang, et al.. "Terahertz master-oscillator power-amplifier quantm cascade laser with grating coupler of extremely low reflectivity". *Opt. Express*, 26, 1942-1953 (2018).

[17] S. Menzel, L. Diehl, C. Pflugl, et al.. "Quantum cascade laser master-oscillator power-amplifier with 1.5 W output power at 300 K". *Opt. Express*, 19, 16229-16235 (2011).

[18] J. Xu, J. M. Hensley, D. B. Fenner, et al.. "Tunable terahertz quantum cascade lasers with an external cavity". *Appl. Phys. Lett.*, 91, 121104 (2007).

[19] L. Nahle, J. Semmel, W. Kaiser, et al.. "Tapered quantum cascade lasers". *Appl. Phys. Lett.*, 91, 181122 (2007).

[20] Y. Y. Li, J. Q. Liu, F. Q. Liu, et al.. "High-performance operation of distributed feedback terahertz quantum cascade lasers". *Electron. Lett*., 52, 945-947(2016).

[21] H. Kogelnik and C. Shank. *J. Appl. Phys*, 43, 2327-2335 (1972).

[22] F. Y. Zhao, Y. Y. Li, J. Q. Liu, et al.. "Sampled grating terahertz quantum cascade lasers". *Appl. Phys. Lett*., 114, 141105(2018).